Inorganic Chemistry

Article

pubs.acs.org/IC

Carbazole-Substituted Iridium Complex as a Solid State Emitter for Two-Photon Intravital Imaging

Marc Lepeltier,[*,†] Florence Appaix,[‡] Yuan Yuan Liao,[§] Frédéric Dumur,[∥] Jérôme Marrot,[†] Tangui Le Bahers,[§] Chantal Andraud,[§] and Cyrille Monnereau[*,§]

[†]Institut Lavoisier de Versailles, UMR 8180 CNRS, Université de Versailles Saint-Quentin en Yvelines, 45 avenue des Etats-Unis, 78035 Cedex Versailles, France

[‡]Univ. Grenoble Alpes, Grenoble Institut des Neurosciences, GIN, Inserm, U1216, F0-38000 Grenoble, France

[§]Laboratoire de Chimie, ENS de Lyon, CNRS UMR 5182, Université Claude Bernard, Université de Lyon, F69342 Lyon, France

[∥]Aix-Marseille Université, CNRS, Institut de Chimie Radicalaire ICR, UMR 7273, F-13397 Marseille, France

Supporting Information

ABSTRACT: A *tris*-cyclometalated iridium complex that bears two ligands functionalized by peripheral carbazole groups combines an intense solid state emission and a significant two-photon absorption cross section in the near-infrared. After incorporation into a physiological micellar suspension, it can be used for the intravital two-photon fluorescence microscopy of cerebral vasculature.

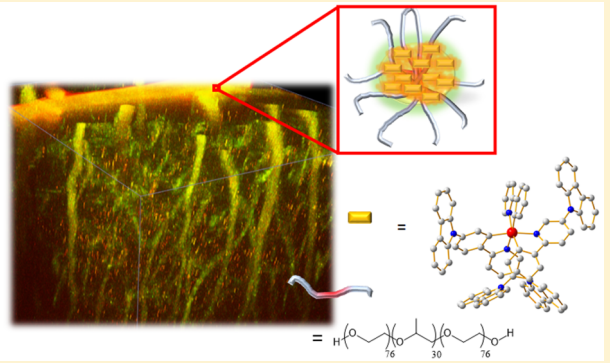

INTRODUCTION

Cyclometalated complexes of the third row transition metals are ubiquitously used in material science, owing to their unmatched luminescence properties.[1] These properties make them particularly valuable components in the fabrication of OLEDs, where some complexes have been shown to display phosphorescence quantum yields close to unity in the solid state.[2]

More recently cyclometalated complexes of Pt and Ir have also been used as fluorescent probes in the framework of confocal or two-photon fluorescence microscopy and bioimaging.[3] To date, their use remain relatively scarce, although constantly expanding.[4] Yet, cyclometalated complexes may offer some significant advantages compared with their organic counterparts:[4a,5] first, their phosphorescence is associated with long lifetimes and large Stokes shifts, two beneficial features to obtain highly contrasted pictures;[6] second their phosphorescence efficiency is known to be little sensitive to photobleaching,[7] a major shortcoming of many fluorescent organic bioprobes;[8] third their lowest lying electronic transition has a mixed intraligand/metal to ligand charge transfer character (ILCT/MLCT).[9] This feature can be used to improve the nonlinear optical response and obtain significant two-photon absorptions at relevant wavelengths (i.e., in the biological transparency window, 700−1000 nm) even with short π-conjugated structures, as illustrated recently with different ruthenium or iridium based chromophores.[10]

However, keeping the luminescence efficiency of such complexes high in a biological environment remains challenging: solubilization of the complex in oxygenated physiological media often results in partial or total quenching of its luminescence because of energy transfer from the long-lived triplet excited state of the complex to molecular oxygen.[11] This phenomenon was very recently used by Lemercier, Natrajan, and co-workers to make a cyclometalated iridium complex-based two-photon sensitizer for photodynamic therapy.[12] Yet, it represents a major shortcoming in the framework of two-photon imaging. Consequently only a few recent examples report the use of such cyclometalated iridium complexes as two-photon probes for bioimaging.[13]

In this paper, we report on a carbazole-substituted *tris*-cyclometalated iridium complex, $Ir(ppy)(cppy)_2$ (Figure 1), with a high solid state luminescence efficiency. This compound presents a characteristic mixed ILCT/MLCT transition at the blue edge of the visible spectrum. Its luminescence, which is highly oxygen sensitive when dissolved in organic solvent, is fully preserved in the solid state. Upon integration in water-dispersed pluronic diblock copolymer micelles, a colloidally stable micellar suspension is formed. We show that the resulting aqueous suspension can be excited by two-photon irradiation in the ILCT/MLCT band with a significant two-

Received: May 24, 2016

ACS Publications © XXXX American Chemical Society

DOI: 10.1021/acs.inorgchem.6b01253
Inorg. Chem. XXXX, XXX, XXX−XXX

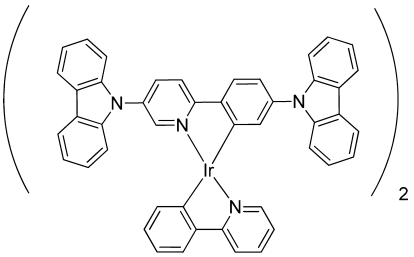

Figure 1. Structure of Ir(ppy)(cppy)$_2$ complex.

photon absorption cross-section. This feature makes this iridium complex a valuable probe for two-photon fluorescence microscopy, as we illustrate with the example of an intravital two-photon microscopy imaging of mouse cerebral vasculature.

EXPERIMENTAL SECTION

Materials and Methods: Synthesis and Characterizations. All commercially available starting materials and solvents were purchased from Aldrich or Lumtec and used as supplied. Pluronic F127 (M_n = 12 500 Da) was supplied from Aldrich. ^{1}H and ^{13}C NMR spectra were determined at room temperature in 5 mm o.d. tubes on a Bruker Avance 300 spectrometer equipped with a QNP probe head: ^{1}H (300 MHz) and ^{13}C (75 MHz). The ^{1}H chemical shifts were referenced to the solvent peak: $CDCl_3$ (7.26 ppm), and the ^{13}C chemical shifts were referenced to the solvent peak: $CDCl_3$ (77.0 ppm). Mass spectroscopy (HRMS) was performed at ILV (Institut Lavoisier de Versailles) of the University of Versailles, St Quentin. Electrospray ionization (ESI) mass spectral analyses were recorded in positive mode with a Xevo QTOF (WATERS) mass spectrometer with a capillary tension of 4500 V, a source temperature of 180 °C, and a cone tension of 60 V.

Dynamic light scattering (DLS) experiments were carried out on a MALVERN zetasizer nano ZS. Samples were irradiated with a helium−neon laser at a working wavelength λ = 632.8 nm. Intensity fluctuations of the scattered light (detected at a backscattering angle of 173°) were fitted using an autocorrelation function. The average particle size and polydispersity index were extrapolated by cumulant analysis using a regularization scheme by intensity, volume, and number.

Crystal Structure Resolution. X-ray intensity data were collected on a Bruker D8 VENTURE diffractometer equipped with a PHOTON 100 CMOS bidimensional detector using a high brilliance IμS microfocus X-ray Mo Kα monochromatized radiation (λ = 0.71073 Å).

Nine sets of narrow data frames (75 s per frame) were collected using at different values of θ for one and eight initial values of ϕ and ω, respectively, using 1° increments of ϕ or ω. Data reduction was accomplished using SAINT, v8.34.[14]

The absorption corrections were based on multiple and symmetry-equivalent reflections in the data sets using the SADABS program[15] based on the method of Blessing.[16] The structure was solved by direct methods and refined by full-matrix least-squares using the SHELX-TL package.[17] Hydrogen atoms were included in calculated positions and allowed to ride on their parent atoms.

Crystal structure analysis: $C_{81}H_{52}Ir_1N_7$, M_w = 1315.49, monoclinic, space group $P2_1$; dimensions a = 13.7778(5) Å, b = 16.8338(7) Å, c = 14.1650(6) Å, β = 116.862(2)°, V = 2930.8(2) Å^3; Z = 2; μ = 2.33 mm^{-1}; 133 761 reflections measured at 200 K; independent reflections 17 184 [15 493 $F_o > 4\sigma(F_o)$]; data were collected up to a $2\theta_{max}$ value of 60.2° (99.8% coverage). Number of variables: 802; R_1 = 0.024, wR_2 = 0.052, S = 1.16; highest residual electron density 0.50 e·Å^{-3}; CCDC 1478156.

Spectroscopy. UV−visible spectra were recorded on a Jasco V-670 spectrophotometer in diluted solutions prepared with solvents of spectroscopic grade. For molar extinction coefficient determination, concentrations were adjusted to 10^{-5} mol L^{-1}. Luminescence spectra were measured using a Horiba-Jobin-Yvon Fluorolog-3 spectrofluorimeter, equipped with a three-slit double-grating excitation and emission monochromator with dispersions of 2.1 nm·mm^{-1} (1200 grooves·mm^{-1}). In the visible range [400−845 nm], the R928 detector was used. Spectra were reference corrected for both the excitation source light intensity variation (lamp and grating) and the emission spectral response (detector and grating). Fluorescence quantum yields in solution, Q, were measured in diluted chloroform solutions with an absorbance lower than 0.1 using the relative method (comparison with a reference compound), according the following approximated equation:

$$Q_x/Q_r = [A_r(\lambda)/A_x(\lambda)][n_x^2/n_r^2][D_x/D_r]$$

where A is the absorbance at the excitation wavelength (λ), n is the refractive index, and D is the integrated luminescence intensity; "r" and "x" stand for reference and sample. Here, reference was coumarine 153 in MeOH (Q_r = 0.45).

Solid state fluorescence spectra were obtained on the same Fluorolog spectrometer as in solution, equipped with a GMP G8 integration sphere. Sample was placed in an open capillary quartz tube, which was inserted into the sphere. Solid state quantum yields were obtained using the methodology originally described in full by De Mello and co-workers.[18] In order to minimize differences between the peak intensities of the lamp and emission profiles and ensure that the collected signal remained in the linear range of the detector, density filters (0.5%) were used to attenuate the intensity of the lamp profile.

Fluorescence lifetime measurements were performed in chloroform at 290 K, using the Horiba-DataStation software on a Horiba-Jobin-Yvon Fluorolog-3 spectrofluorimeter, equipped with a NanoLED 390 source operating at 390 nm with 1.2 ns pulses, a iHR320 emission monochromator with 1200 grooves·mm^{-1} gratings and an R928 detector. The fluorescence decay signal was reconstructed from time correlated single photon counting (TCSPC) and deconvoluted using the Decay Analysis Software (DAS)

The TPA cross-section spectra were obtained by two-photon excited fluorescence measurement of a 10^{-4} M aqueous suspension of Ir(ppy)(cppy)$_2$ in pluronic, using a Ti:sapphire mode-locked femtosecond laser (Spectra Physics Inc., USA), with a pulse duration of 100 fs and a repetition rate of 82 MHz as an excitation source. The excitation beam (5 mm diameter) was focused with a lens (focal length 10 cm) at the middle of the fluorescence cell (10 mm). The fluorescence, collected at 90° to the excitation beam, was focused into an optical fiber (diameter 600 μm) connected to an Ocean Optics S2000 spectrometer. After passing through a short-pass filter to remove the pump after 700 nm, the incident beam intensity was adjusted to 110 mW in order to ensure an intensity-squared dependence of the fluorescence over the whole spectral range and quadratic dependence of the TPA on the excitation intensity was checked to exclude possible artifacts. The detector integration time was fixed to 1 s. Calibration of the spectra was performed by comparison with the published 700−900 nm Coumarin-307 and fluorescein two photon absorption spectra.[19]

Imaging. In accordance with the policy of Grenoble Institute of Neuroscience (GIN) and the French legislation, experiments were done in compliance with the European Community Council Directive of November 24, 1986 (86/609/EEC). The research involving animals was authorized by the Direction Départementale des Services Vétérinaires de l'Isère − Ministère de l'Agriculture et de la Pêche, France, and the Direction Départementale de la protection des populations - Préfecture de l'Isère-France (F. Appaix, Ph.D., permit number 38 09 39). All efforts were made to minimize the number of mice used and their suffering during the experimental procedure. CD1 mice were housed in cages with food and water ad libitum in a 12 h light/dark cycle at 22 ± 1 °C.

For in vivo two-photon laser scanning microscopy (TPLSM), a 4-month-old CD1 mouse was anesthetized using isoflurane (5% for induction and 1−2% during experiments) in a 70% air/30% O_2 gas mixture. Its body temperature was monitored with a rectal probe and maintained at 36 °C using a heating blanket. A craniotomy of 2−3 mm in diameter was performed with a dental drill above the motor cortex and filled with ultrasound gel.

DOI: 10.1021/acs.inorgchem.6b01253
Inorg. Chem. XXXX, XXX, XXX−XXX

Scheme 1. Synthesis of cppy

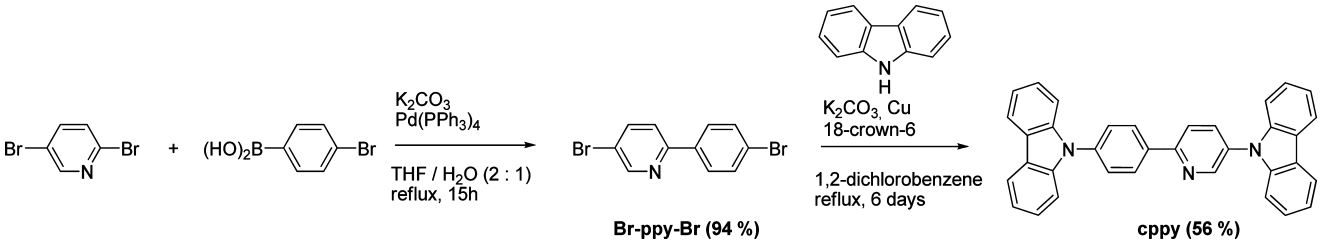

A catheter (NeoflonTM, BD, USA) was inserted in the tail vein for an intravenous (iv) injection of 0.1 mL of the pluronic suspension of $Ir(ppy)(cppy)_2$ in saline just before the imaging experiments.

TPLSM was performed using a LSM 7MP (Zeiss, Germany) equipped with a 20× water-immersion objective (NA 1.0; Zeiss) and ZEN 2010 software. Fluorescence light emission was collected in the epifluorescence configuration using two high sensitivity non-descanned detectors (GaAsP) in the epi-collection mode. A dichroic beamsplitter FF562 was used to split the phosphorescence emission with a FF01 617/73 nm filter for the red channel and a FF01 542/50 nm filter for the green channel (Semrock, US).

Laser excitation at 780 nm was done using a Ti:sapphire laser (Chameleon Vision II; Coherent, UK). All the TPLSM images were obtained with less than 50 mW laser power at the cortical surface. Three-dimensional two-photon microscopy images were acquired as *z*-stacks with 425 μm × 425 μm *X*−*Y* plane size and a 3 μm step size between each focus plane. The *z*-projections were performed with ImageJ software,[20] and Vaa3D software was used for 3D image reconstruction.[21]

Computational Details. Molecular calculations were carried out with the Gaussian09 code.[22] The global hybrid functional PBE0 was used for both ground state and excited state calculations.[23] This functional has been chosen because it has recently been proven to yield reliable valence charge transfer excitations in inorganic complexes.[24] Structural optimizations and subsequent frequency calculations for the ground state were performed using an all electron Pople double-ζ basis set with one polarization on heavier atoms (6-31G(d)) for C, N, and H atoms and using the Los Alamos pseudopotential and associated double-ζ basis set (LANL2DZ) for Ir atom.[25] All optimizations were performed by including the D3 Grimme dispersion correction with the Becke−Johnson damping.[26] The first 30 vertical singlet−singlet excitations were computed by the means of TD-DFT using the 6-31+G(d) basis set on C, N, and H atoms. The next 20 excitations were computed using the 6-31G(d) basis set on C, N, and H atoms to save computational time. The first singlet−triplet absorption band was computed by TD-DFT with the 6-31+G(d) basis within the Tamm−Dancoff approximation that has proven its reliability to compute the singlet−triplet gaps.[27] The phosphorescence energy was computed by optimizing the first triplet state with a ΔSCF procedure using the 6-31G(d) basis set followed by a TD-DFT singlet−triplet vertical excitation calculation in the Tamm−Dancoff approximation. Bulk solvent effects were included using the polarizable continuum model (PCM) of Tomasi and co-workers.[28] More specifically, the conductor-like PCM model as implemented in Gaussian (CPCM) was applied, and chloroform was considered as solvent in analogy with the experimental medium.[29] Default radii (from the UFF, scaled by 1.1) were used for structural optimizations. The charge transfer distance, noted d_{CT}, is computed from the variation of the electron density map using equations presented in refs 24 and 30 and tested on complexes. Vibrationally resolved spectra were obtained after performing frequency calculations (analytically and numerically for the ground and excited states, respectively) using the FCclasses program.[31] The reported spectra were simulated at 0 K using convolutions with Gaussian functions presenting a fwhm of 0.05 eV. Twenty-five overtones for each mode, 20 combination bands, and a maximum of 10^9 integrals for each class were used.

Synthetic Procedures. *5-Bromo-2-(4-bromophenyl)pyridine (Br-ppy-Br).* To a solution of 2,5-dibromopyridine (5.0 g, 21.3 mmol) and 4-bromophenylboronic acid (4.26 g, 21.3 mmol) in tetrahydrofuran (THF, 100 mL) was added tetrakis-(triphenylphosphine)palladium (0.62 g, 0.53 mmol). The reaction mixture was stirred at 50 °C for 30 min. Then, a solution of sodium carbonate (6.77 g, 63.8 mmol) in water (50 mL) was added, and the reaction mixture was refluxed during 15 h. After cooling to room temperature, THF was evaporated, and the product was extracted with ethyl acetate (3 × 100 mL). The organic phase was then washed with brine (100 mL) and dried over $MgSO_4$, and the solvent was evaporated. The product was purified by column chromatography on silica gel using dichloromethane/petroleum ether (50:50) as eluent and was recovered as a white powder (6.25 g, 94%). ^{1}H NMR (300 MHz, $CDCl_3$): 8.74 (d, ^4J = 2.4 Hz, 1H), 7.87 (m, 3H), 7.61 (m, 3H). ^{13}C NMR (75 MHz, $CDCl_3$): 154.7, 150.4, 139.4, 137.1, 132.0, 128.3, 123.9, 121.3, 119.7. MS (ESI) Calcd for $C_{11}H_7Br_2N$ 312.99; Found 313.9008 $[M + H]^+$.

9-(6-(4-(9H-Carbazol-9-yl)phenyl)pyridin-3-yl)-9H-carbazole (cppy). To a solution of 5-bromo-2-(4-bromophenyl)pyridine (2.0 g, 6.39 mmol) in 1,2-dichlorobenzene (50 mL) were added carbazole (3.2 g, 19.2 mmol), potassium carbonate (7.05 g, 51.1 mmol), copper (1.62 g, 25.6 mmol), and 18-crown-6 (0.34 g, 1.28 mmol). The reaction mixture was refluxed for 6 days. Then, the solvent was evaporated. A saturated ammonium chloride solution in water (100 mL) was added, and the product was extracted with dichloromethane (3 × 100 mL). The organic phase was then dried over $MgSO_4$, and the solvent was evaporated. The product was purified by column chromatography on silica gel using dichloromethane/petroleum ether from 1:4 to 1:1 as eluent to be isolated as a white powder (1.75 g, 56%). ^{1}H NMR (300 MHz, $CDCl_3$): 9.5 (d, ^4J = 1.8 Hz, 1H), 8.37 (d, ^3J = 8.4 Hz, 2H), 8.21 (dd, ^3J = 8.1 Hz, ^4J = 3.0 Hz, 4H), 8.08 (m, 2H), 7.79 (d, ^3J = 8.4 Hz, 2H), 7.52 (m, 8H), 7.37 (m, 4H). ^{13}C NMR (75 MHz, $CDCl_3$): 155.2, 148.3, 140.74, 140.70, 138.8, 137.4, 135.2, 133.5, 128.5, 127.4, 126.4, 126.1, 123.9, 123.7, 121.1, 120.7, 120.6, 120.4, 120.2, 109.9, 109.5. MS (ESI) Calcd for $C_{35}H_{23}N_3$ 485.1965; Found 486.1964 $[M + H]^+$.

Ir(C^N)$_2$Cl$_2$Ir(C^N)$_2$. $Ir(C^N)_2Cl_2Ir(C^N)_2$ was synthesized by a method modified from a literature procedure.[32] To a solution of HC^N (ppy or cppy) (3.0 mmol) in 2-ethoxyethanol/water (75:25, 50 mL) was added $IrCl_3 \cdot 3H_2O$ (1.2 mmol). The reaction mixture was stirred at reflux for 24 h. Then, water (50 mL) was added, and the product was filtered and washed with ethanol (50 mL) and diethyl ether (50 mL). The product was then isolated as a powder. $Ir(ppy)_2Cl_2Ir(ppy)_2$, yellow powder, 89%. ^{1}H NMR (300 MHz, $CDCl_3$): 9.25 (d, ^3J = 5.4 Hz, 4H), 7.88 (d, ^3J = 8.1 Hz, 4H), 7.75 (dt, ^3J = 7.2 Hz, ^4J = 1.5 Hz, 4H), 7.50 (dd, ^3J = 7.8 Hz, ^4J = 1.2 Hz, 4H), 6.77 (m, 8H), 6.57 (dt, ^3J = 7.8 Hz, ^4J = 0.9 Hz, 4H), 5.94 (d, ^3J = 7.5 Hz, 4H). $Ir(cppy)_2Cl_2Ir(cppy)_2$, yellow powder, 96%. The latter complex being insoluble in all tested NMR solvents, it was directly engaged in the next step of the reaction.

Ir(ppy)(cppy)$_2$. Method 1, to a solution of 9-(6-(4-(9*H*-carbazol-9-yl)phenyl)pyridin-3-yl)-9*H*-carbazole (2.14 g, 4.52 mmol) in 2-ethoxyethanol (40 mL) was added silver triflate (1.45 g, 5.64 mmol) and $Ir(ppy)_2Cl_2Ir(ppy)_2$ (2.42 g, 2.28 mmol). Method 2, to a solution of 2-phenylpyridine (26 mg, 0.167 mmol) in 2-ethoxyethanol (10 mL) was added silver triflate (54 mg, 0.21 mmol) and $Ir(cppy)_2Cl_2Ir(cppy)_2$ (0.2 g, 0.0836 mmol). In both cases, the reaction mixture was refluxed for 36 h. After cooling to room temperature, the solvent was evaporated, water (100 mL) was added, and the product was extracted

DOI: 10.1021/acs.inorgchem.6b01253
Inorg. Chem. XXXX, XXX, XXX−XXX

Scheme 2. Synthesis of $Ir(ppy)_2(cppy)$ and $Ir(ppy)(cppy)_2$

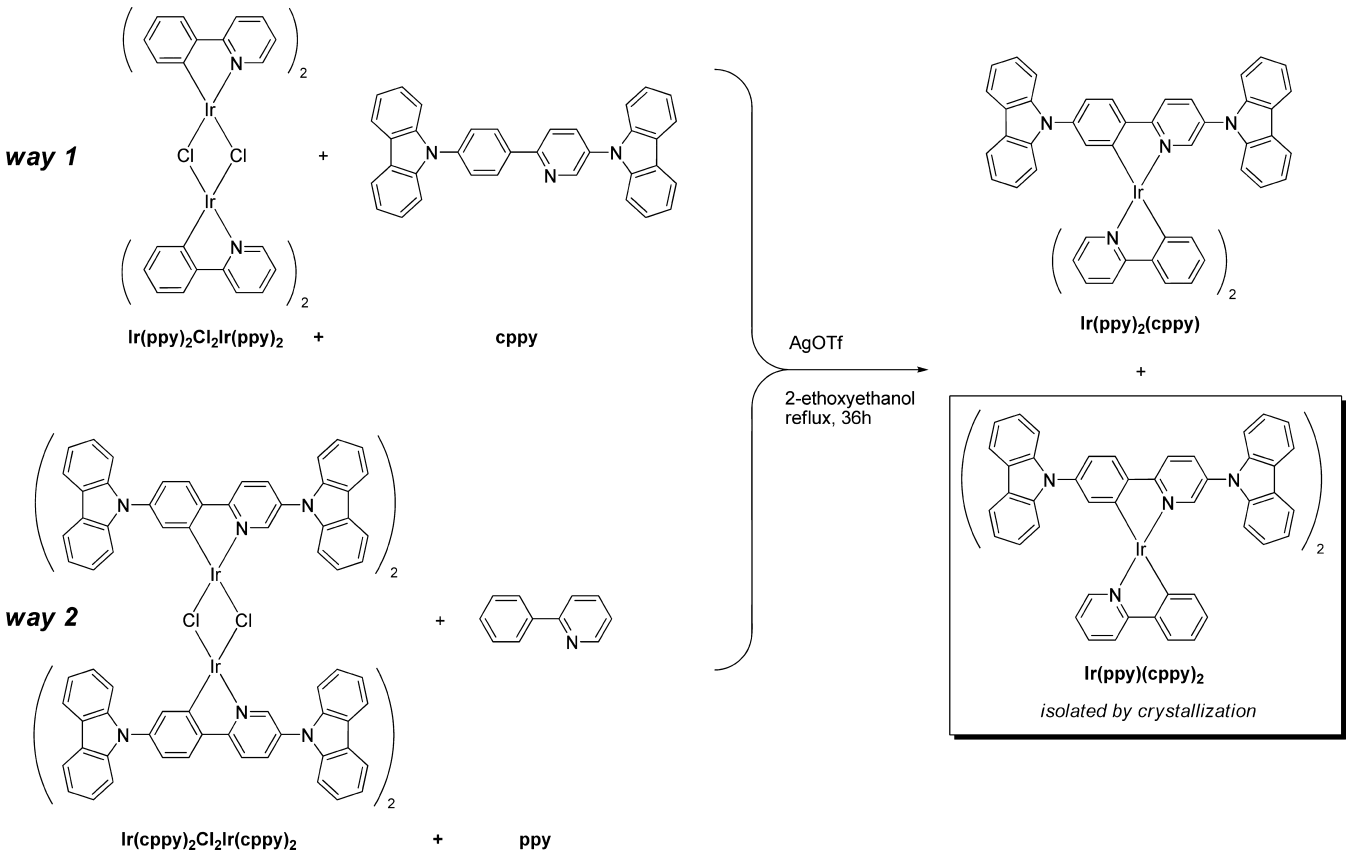

with dichloromethane (3 × 100 mL). The organic phase was then dried over $MgSO_4$, and the solvent was evaporated. A mixture of $Ir(ppy)_2(cppy)$ and $Ir(ppy)(cppy)_2$ was isolated by chromatography on silica gel using dichloromethane/petroleum ether from (1:4) to (1:1) as eluent. Then $Ir(ppy)(cppy)_2$ was isolated by crystallization by slow diffusion of diethyl ether in a solution of the mixture in dichloromethane to be isolated as a yellow powder (method 1, 1.49 g, 50%; method 2, 13 mg, 6%). ^{1}H NMR (300 MHz, $CDCl_3$): 8.19 (m, 5H), 8.06 (m, 9H), 7.90 (m, 3H), 7.80 (m, 2H), 7.56 (m, 3H), 7.39 (m, 2H), 7.34 (m, 2H), 7.28 (m, 4H), 7.15 (m, 18H), 6.80 (m, 2H), 6.79 (m, 2H). MS (ESI) Calcd for $C_{81}H_{52}IrN_7$ 1315.3922; Found 1315.4198 $[M]^{+\cdot}$.

RESULTS AND DISCUSSION

Synthesis. The synthetic route toward the $Ir(ppy)(cppy)_2$ complex is outlined in Schemes 1 and 2. Briefly, the precursor Br-ppy-Br was obtained almost quantitatively by palladium-catalyzed Suzuki coupling between the 2,5-dibromopyridine and 4-bromophenylboronic.[33] Only the coupling on the 2-position of 2,5-dibromopyridine was observed. Then, the cppy compound was prepared in reasonable yield (56%) by copper-catalyzed Ullman condensation with carbazole in the presence of crown ether.[34]

Finally, the complex $Ir(ppy)(cppy)_2$ was synthesized following published procedures.[35] The dimer $Ir(ppy)_2Cl_2Ir(ppy)_2$ was reacted with silver triflate to afford coordination of the third ligand (cppy) to the iridium center. It appeared that under these reaction conditions, not only one single cppy had been introduced on the metal center to form the $Ir(ppy)_2(cppy)$ complex, but this coordination has been followed by an exchange of a ppy ligand with another cppy leading to the formation of the complex $Ir(ppy)(cppy)_2$. This ligand exchange process had already been reported with fluorinated phenylpyridine ligands.[36] High resolution mass spectroscopy (HRMS) confirmed the composition of the mixture with the presence of two peaks at m/z = 985.2765 for $Ir(ppy)_2(cppy)$ and at m/z = 1315.4198 for $Ir(ppy)(cppy)_2$. We were unable to obtain the $Ir(ppy)(cppy)_2$ by modifying the reaction conditions (i.e., by reacting the precursor $Ir(ppy)_2Cl_2Ir(ppy)_2$ with excess cppy or by refluxing the reaction mixture for longer time). Purification by column chromatography was unsuccessful because their polarities are too similar. The same mixture of $Ir(ppy)_2(cppy)$ and $Ir(ppy)(cppy)_2$ was obtained by reacting the dimer $Ir(cppy)_2Cl_2Ir(cppy)_2$ with ppy (method 2). Although it appeared impossible to synthesize pure $Ir(ppy)_2(cppy)$ and $Ir(ppy)(cppy)_2$ from published procedures, the presence of two additional carbazole groups on the $Ir(ppy)(cppy)_2$ decreased its solubility, and this complex was crystallized by slow diffusion of diethyl ether into a dichloromethane solution in better yield with method 1 (50% yield against 6% yield for method 2).

Crystallography. Monocrystals of $Ir(ppy)(cppy)_2$ suitable for X-ray diffraction were obtained by slow diffusion of cold diethyl ether into a solution of the mixture of $Ir(ppy)_2(cppy)$ and $Ir(ppy)(cppy)_2$ in dichloromethane. The complex $Ir(ppy)(cppy)_2$ (CCDC 1478156) exhibits a pseudo-octahedral geometry around the iridium center (Figure 2). Examination of the crystal structure reveals a significantly distorted π-conjugated backbone for the two cppy ligands: the phenyl and pyridine rings are not coplanar with a small dihedral angle of 14.32° and 15.81° for each cppy. The carbazole moieties are also tilted with respect to the adjacent phenyl or pyridine ring (dihedral angles from 52.85° to 65.20°). This is probably due to steric repulsions. The smallest distance between the carbon

DOI: 10.1021/acs.inorgchem.6b01253
Inorg. Chem. XXXX, XXX, XXX−XXX

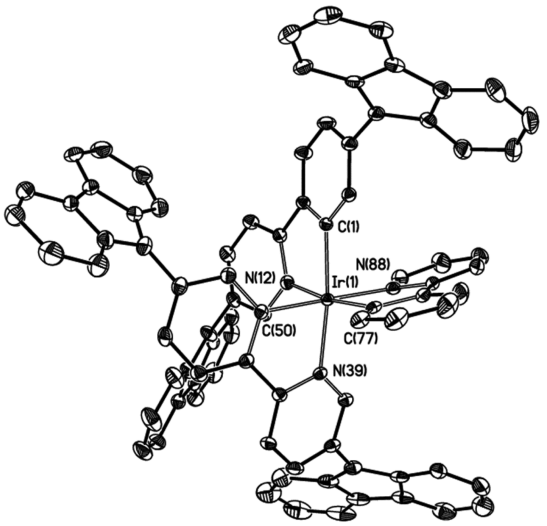

Figure 2. Perspective view of $Ir(ppy)(cppy)_2$, with the 30% probability thermal ellipsoid. Hydrogen atoms have been removed for clarity.

atoms of ppy and the closest carbazole is only 3.75 Å with 3.96 Å between the two closest carbazoles. These distances are in agreement with the hypothesis of a marked steric hindrance in the complex, similar to what has been previously reported on cationic iridium(III) complexes with bipyridine ligands substituted with tilted phenyl rings.[37]

Spectroscopy. Spectroscopic properties of $Ir(ppy)(cppy)_2$ were investigated in a diluted chloroform solution (Figure 3a). $Ir(ppy)(cppy)_2$ displays a very typical UV−vis absorption spectrum for this class of complexes. It features a dominant absorption in the UV, which can be classically ascribed to a $\pi-\pi^*$ transition centered on the phenylpyridine cyclometalated ligands. A lower intensity transition is centered at 350 nm with a shoulder around 400 nm and broad tail in the 450−500 nm region. TD-DFT calculations reproduce the shape of the absorption spectrum in the 300−500 nm region indicating that several electronic transitions are involved in this band. The shoulder at 400 nm is not a vibronic evolution of the band at 350 nm but comes from two independent transitions having a MLCT character (see Figure 4b) with a small computed charge transfer distance, $d_{CT} \approx 1.9$ Å. The band at 350 nm is dominated by two transitions having a mixed ILCT and MLCT character (Figure 4c) with a longer charge transfer distance, $d_{CT} \approx 3.2$ Å. Finally, the broad tail around 450−500 nm could be due to singlet−triplet MLCT transitions, induced by heavy element effect (as illustrated by the first four singlet−triplet transitions computed by TD-DFT and presented in Figure 3b). From the emission point of view, the dominant band, centered at 525 nm, also exhibits a typical ^{3}MLCT character as confirmed by the TD-DFT simulated vibronically resolved phosphorescence spectrum (dashed black line, Figure 3b). This emission has a marked vibronic progression and large Stokes shift (9700 cm^{-1}). The emission quantum yield, which is below 0.03 in oxygenated chloroform solution, increases to 0.75 upon degassing, which further supports the triplet nature of the associated excited state and the fact that it is efficiently quenched by molecular oxygen (Figure S1).

Luminescence shows an almost perfect monoexponential decay ($r^2 > 0.998$). This might at first sight appear counterintuitive, because such a *tris*-cyclometalated complex should indeed coexist as two distinct configuration isomers,

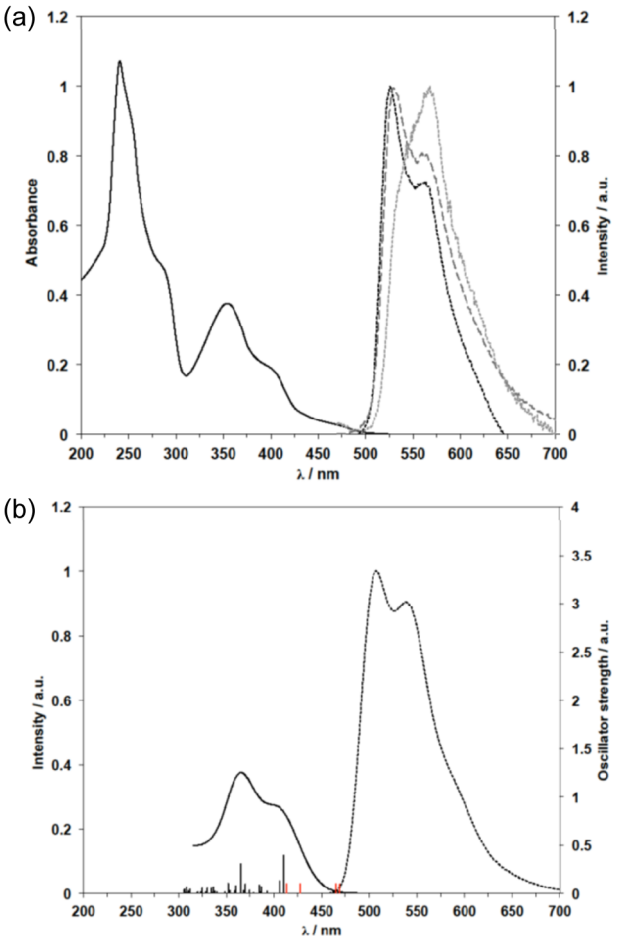

Figure 3. (a) Absorption spectrum (black solid line) and emission spectra (λ_{ex} = 390 nm) of complex $Ir(ppy)(cppy)_2$ as a 2.5×10^{-5} M solution in chloroform (black dotted line), in the solid state (gray dotted line), and in pluronic micelles (gray dashed line). (b) TD-DFT computed 50 first singlet−singlet excitations (vertical black lines) and the first four singlet−triplet excitations (vertical red lines, arbitrary low oscillator strengths were used for the drawing, and those were not included in the simulated absorption spectrum). The absorption spectrum was simulated up to 310 nm (black solid line) and was obtained by convoluting the TD-DFT excitations with gaussians (fwhm of 0.35 eV). The simulated phosphorescence spectrum including vibronic coupling is in dashed black line.

namely facial (*fac*) and meridional (*mer*); it has been well documented in the literature that both configurations present a very distinctive luminescence lifetime, with an average (*mer*) 10 times shorter than its (*fac*) counterpart, and a mixture of both should lead to a multicomponent decay. The fact that a single lifetime component of 1.3 μs is seen, which is an average value for ^{3}MLCT phosphorescence processes in such cyclometalated iridium complexes,[38] suggests that only one of the two species is formed (Figure 5). This can be explained on the basis of the significant difference in the thermodynamic stability between the two complexes and of the kinetic lability of the ligands, which progressively drives the system to its thermodynamically most stable isomer upon prolonged heating. This assumption is supported by DFT calculations performed on the facial and the two meridional isomers. The facial conformer is computed to be more stable by ~30 kJ mol^{-1} indicating that thermodynamically almost all the molecules should be in the facial form at room temperature in good agreement with our observation.

DOI: 10.1021/acs.inorgchem.6b01253
Inorg. Chem. XXXX, XXX, XXX−XXX

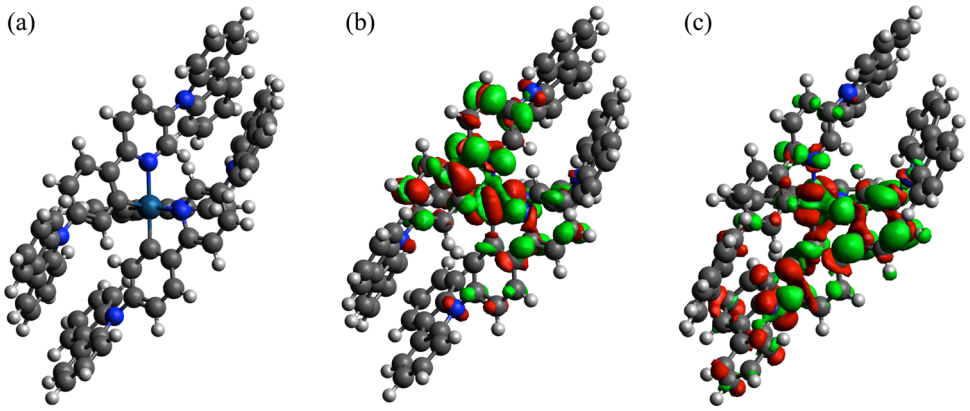

Figure 4. (a) Ir(ppy)(cppy)$_2$ structure optimized by DFT. (b, c) Computed electron variation density between the ground and excited states of the most intense transitions of the 400 and 350 nm bands, respectively. The red and green zones correspond to the regions where the electron density is decreasing and increasing, respectively, upon excitation, evidencing a MLCT and mixed MLCT/ILCT for panels b and c, respectively (isovalue 0.0006 au).

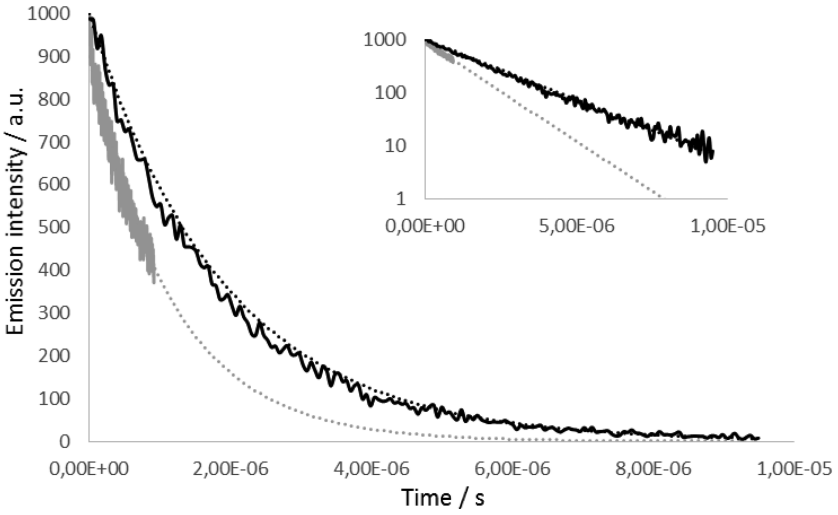

Figure 5. Emission decay (solid line) and monoexponential fit (dotted) of Ir(ppy)(cppy)$_2$ in chloroform (2.5×10^{-5} M, black) and at the solid state (gray). Inset shows the same data with intensity axis in logarithmic scale (λ_{ex}, 390 nm; λ_{em}, 590 nm).

The excitation spectrum of the phosphorescence band is overall superimposable to the absorption one, although the low-energy shoulder of the ILCT/MLCT band is a little less prominent on the former (Figure S2).

Emission and excitation spectra of a powder sample of Ir(ppy)(cppy)$_2$ were recorded in an integrating sphere.[39] In good consistency with literature data on related complexes,[40] the recorded solid-state emission is very similar in position of the maxima and general band shape to the one measured in solution, although the vibronic progression is blurred and the dominant transition is no more the $\nu_0^* \rightarrow \nu_0$ but the $\nu_0^* \rightarrow \nu_1$ (Figure 3a). The emission quantum yield (0.40) is slightly reduced compared to solution data but does not show any significant dependence on the presence of oxygen. Emission lifetime undergoes a similar evolution as it drops to 0.77 μs in the solid state (Figure 5). This is clear evidence that an increase of nonradiative kinetics is mainly responsible for the decrease of emission efficiency between the solution ($k_r = 5.2 \times 10^5$ s^{-1}; $k_{nr} = 1.9 \times 10^5$ s^{-1}) and the solid state ($k_r = 5.6 \times 10^5$ s^{-1}; $k_{nr} = 7.8 \times 10^5$ s^{-1}).

Preparation and Characterization of Fluorescent Micellar Suspension. A pluronic micellar suspension of Ir(ppy)(cppy)$_2$ in physiological serum was obtained following the protocol schematized in Figure 6. Briefly, dropwise addition of a concentrated solution of Ir(ppy)(cppy)$_2$ (0.4 mg) and pluronic F127 (80 mg) in THF (0.1 mL) into 10 mL of physiological serum stirred at 300 rpm was followed by continuous stirring of the solution until full evaporation of the residual THF (ca. 72 h). Then, the slightly opalescent solution was filtered through 0.45 μM nylon filters, affording a bright, limpid yellowish aqueous suspension. DLS measurement (Figure S3) allowed us to estimate a medium particle size of about 80 nm, with relatively narrow distribution (PDI = 0.2), in good agreement with previous reports on similar pluronic based micellar systems.[41]

Spectroscopic measurements were performed on the resulting micellar suspension of Ir(ppy)(cppy)$_2$. The overall appearance of the absorption and emission spectra are very similar to those of the isolated molecule in deaerated chloroform solutions. However, its quantum yield was significantly lowered, even compared to the solid state sample (0.15; Figure 3a). Such a decrease in fluorescence between the bulk solid state material and micellar suspension has been already evidenced in the past for other solid states luminophores.[42] In good consistency with the luminescence quantum-yield lowering, time-resolved luminescence measure-

DOI: 10.1021/acs.inorgchem.6b01253
Inorg. Chem. XXXX, XXX, XXX−XXX

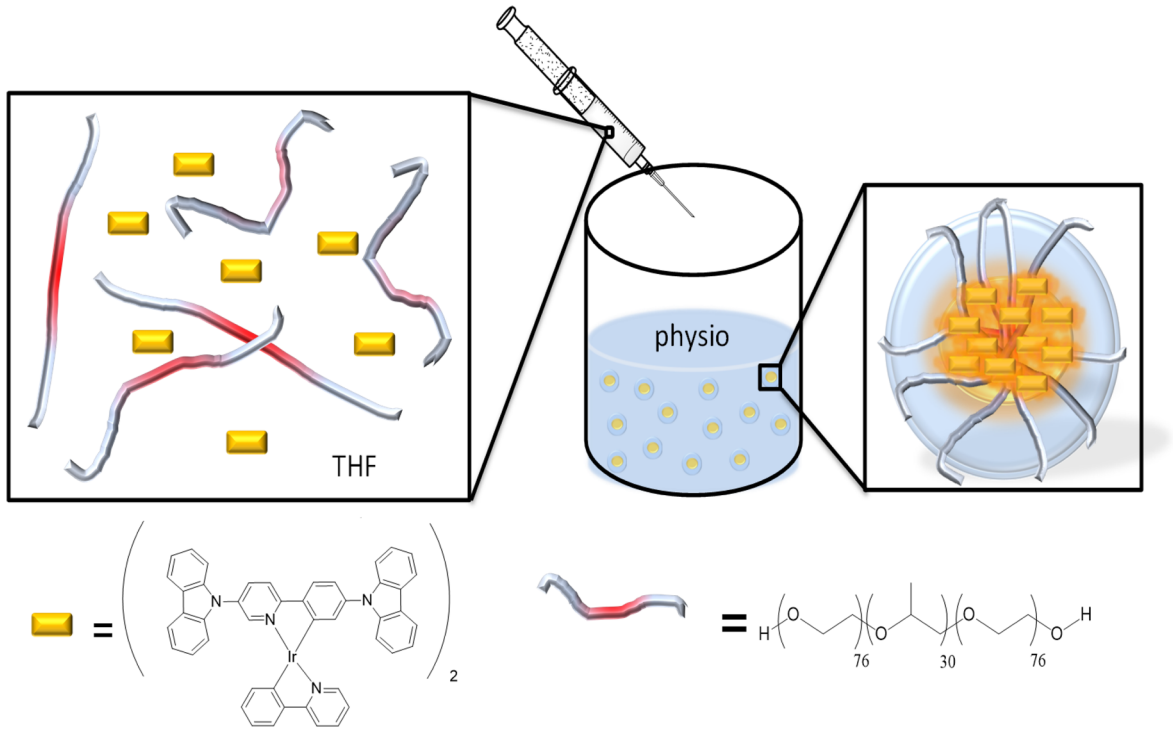

Figure 6. Schematic protocol used for the preparation of micellar suspension of $Ir(ppy)(cppy)_2$ in pluronic in saline.

ments clearly point out a shortening of the luminescence lifetime, along with the involvement of two contributions in the luminescence decay: one dominant (75%) longer lifetime of 0.29 μs along with a minor (25%) shorter contribution of 86 ns (Figure S4). Such a behavior is classically encountered in micellar systems and is generally attributed to differences in chromophore molecule localization within the micelles, peripheral molecules being more directly exposed to water and ions and thus more prone to undergo nonradiative quenching of their luminescence.[43] Measurements conducted in aerated and deaerated solutions unambiguously ascertained the insensitivity of phosphorescence intensity toward oxygen (Figure S1b), which is a clear indication of the solid-state nature of the encapsulated complex and also a very positive feature in view of TPLSM imaging in living organisms. Conversely, it is worth noting that attempts to dissolve $Ir(ppy)(cppy)_2$ alone in water or physiological serum remained unsuccessful, thus clearly evidencing the micellar nature of the obtained suspension. UV–vis measurement of the absorbance of this suspension allowed us to approximate a total chromophore concentration of about 1.1×10^{-4} M (making the assumption of a molar extinction coefficient similar to that of the free chromophore in solution), high enough to make it relevant for intravital fluorescence microscopy, as illustrated in the following.

Two-photon excitation spectrum and cross-section of $Ir(ppy)(cppy)_2$ in micellar suspension were measured by the two-photon induced fluorescence technique (TPIF, Figure 7), details of which are given in the Experimental Section.[44] As a result of a one-photon absorption spectrum located mainly in the UV, we were not able to record the whole two-photon spectrum using our titanium–sapphire based setup, which only spans the 730–950 nm region. In the investigated region of the spectrum, which corresponds to the mixed ILCT/MLCT transition of the complex, a relatively weak though significant

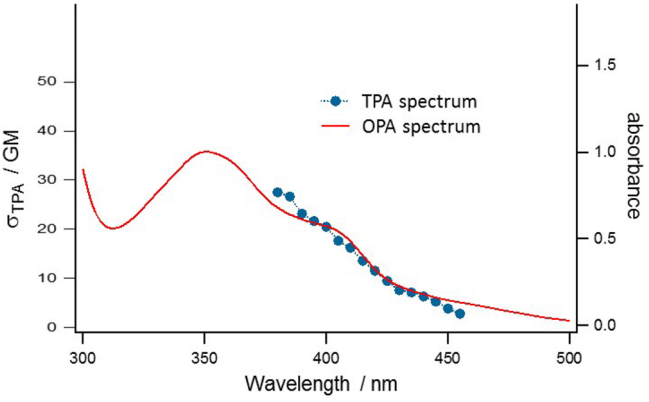

Figure 7. TPE (Two-photon excitation) spectrum (blue circles) overlaid with the OPA (one-photon absorption) spectrum (red solid line) of a micellar suspension of $Ir(ppy)(cppy)_2$/pluronic in physiological serum. The TPE spectrum is plotted at half the original wavelength. σ_{TPA} stands for two-photon absorption cross-section, 1 GM = 10^{-50} (cm^4 s)/photon.

two-photon absorption cross section was measured. The value of σ_{TPA} peaked at 750 nm (30 GM),[45] then gradually decreased upon red-shifting of the excitation. Superimposition of the collected two-photon action spectrum of the micellar suspension with the UV–vis linear absorption spectrum indicates that the excited states involved in OPA and TPA processes are the same. This constitutes clear evidence of the participation of the metal-to-ligand transition from the iridium to the cppy ligand (noncentrosymetric in nature, hence the superimposition) in the nonlinear optical response of the molecule, as already observed in ref 10a.

Intravital Microscopy Imaging. In order to bring evidence for the applicability of the material in the framework of two-photon fluorescence bioimaging, intravital two-photon laser scanning microscopy (TPLSM) experiments were under-

DOI: 10.1021/acs.inorgchem.6b01253
Inorg. Chem. XXXX, XXX, XXX–XXX

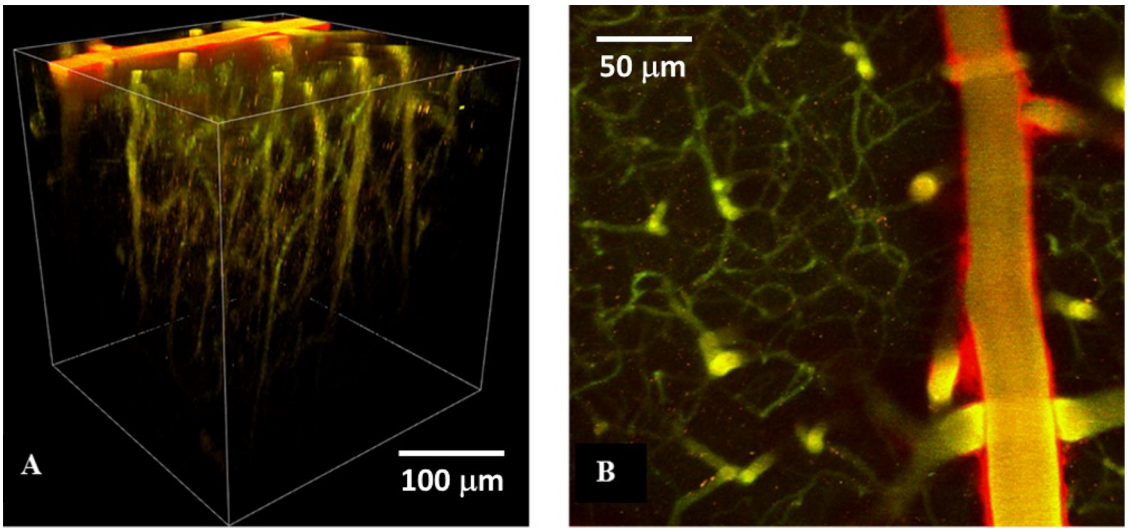

Figure 8. (A) *In vivo* 3D TPLSM (λ_{ex} = 780 nm) image of the cerebral vasculature in an adult mouse, as obtained after iv injection of the Ir(ppy)(cppy)$_2$ micellar suspension. (B) Standard deviation projections of TPLSM z-stacks. A minimal step of 3 μm between the different $x-y$ planes (512 pixels × 512 pixels, 425 μm × 425 μm) using the motorized objective resulting in a maximum observation depth of 400 μm in the motor cortex with a craniotomy of an adult mouse.

taken, following a well-established protocol,[42,46] details of which can be found in the Experimental Section, and using Ir(ppy)(cppy)$_2$ as a two-photon phosphorescent contrast agent.

A small amount (typically 100 μL) of the micellar suspension of phosphorescent Ir(ppy)(cppy)$_2$ was intravenously injected into the mouse tail. Then, tridimensional images of its brain vasculature were recorded by TPLSM through a cranial window. Excitation was performed at 780 nm, a range of wavelength where the transition involved in the two-photon absorption process is of pure ILCT/MLCT character (with a σ_{TPA} of ca. 20−30 GM). Although the collected fluorescence signal was significantly weaker than that generally obtained on similar equipment with state-of-the-art two-photon fluorescent probes specifically designed for this application,[46,47] resulting in a lower signal-to-noise ratio, the details of blood vasculature were clearly evidenced with good contrast, micrometric resolution, and imaging depth up to 400 μm (Figure 8). This result is comparable to other recent reports dealing with aggregated organic chromophore nanoparticles.[48]

CONCLUSIONS

We designed a new type of cyclometalated iridium complex, where two of the ppy ligands were functionalized by two peripheral carbazole donor groups, in order to optimize its nonlinear absorption properties. Its absorption and luminescence properties were characterized through a detailed spectroscopic study. In particular, it was shown that this complex displays an intense ^{3}MLCT phosphorescent band in the orange part of the visible spectrum, both in a deaerated organic solvent solution and in the solid state. Integration of Ir(ppy)(cppy)$_2$ into a colloidal micellar suspension of pluronic in physiological serum afforded a bright yellowish solution with good, oxygen-independent luminescence and significant two-photon absorption properties. This solution was straightaway usable for iv injection, making it possible to image the details of a mouse's brain vasculature using TPSLM. It is worth mentioning that both the two-photon excitation and the emission process occurred to and from electronic states that possess a significant (or even dominant) metal-to-ligand charge transfer character, which constitutes an uncommon feature in the framework of TPLSM microscopy. Contrasted images of high resolution of mice cerebral vasculature were obtained *in vivo*, thus confirming the relevance of this class of coordination compounds, once shielded from the oxygen influence by their incorporation into nanoparticles, for bioimaging applications.

ASSOCIATED CONTENT

Supporting Information

The Supporting Information is available free of charge on the ACS Publications website at DOI: 10.1021/acs.inorgchem.6b01253.

Luminescence spectra of Ir(ppy)(cppy)$_2$ in dichloromethane solution and in the solid state under inert or aerated conditions, absorption and excitation spectrum of Ir(ppy)(cppy)$_2$ in dichloromethane solution, DLS of the nanoparticle solution of Ir(ppy)(cppy)$_2$/pluronic in saline, phosphorescence lifetime measurements of Ir(ppy)(cppy)$_2$ in micellar pluronic suspensions, and summary of the main crystal parameters (PDF)

Crystallographic information for Ir(ppy)(cppy)$_2$ (CIF)

AUTHOR INFORMATION

Corresponding Authors

*E-mail: marc.lepeltier@uvsq.fr.

*E-mail: cyrille.monnereau@ens-lyon.fr.

Author Contributions

The manuscript was written through contributions of all authors. All authors have given approval to the final version of the manuscript.

Notes

The authors declare no competing financial interest.

ACKNOWLEDGMENTS

The authors acknowledge the "Pôle Scientifique de Modélisation Numérique" (PSMN) for provinding computational resources. *In vivo* TPLSM imaging was performed at the Two-Photon Microscopy Platform PIC-GIN (Photonic Imag-

DOI: 10.1021/acs.inorgchem.6b01253
Inorg. Chem. XXXX, XXX, XXX−XXX

ing Center, Grenoble Institute of Neuroscience, GIS-IBiSA ISdV).

REFERENCES

(1) (a) Dixon, I. M.; Collin, J.-P.; Sauvage, J.-P.; Flamigni, L.; Encinas, S.; Barigelletti, F. A family of luminescent coordination compounds: iridium(III) polyimine complexes. *Chem. Soc. Rev.* **2000**, *29* (6), 385−391. (b) Medlycott, E. A.; Hanan, G. S. Designing tridentate ligands for ruthenium(II) complexes with prolonged room temperature luminescence lifetimes. *Chem. Soc. Rev.* **2005**, *34* (2), 133−142. (c) Chen, Z.-q.; Bian, Z.-q.; Huang, C.-h. Functional IrIII Complexes and Their Applications. *Adv. Mater.* **2010**, *22* (13), 1534−1539.

(2) (a) Hu, T.; He, L.; Duan, L.; Qiu, Y. Solid-state light-emitting electrochemical cells based on ionic iridium(III) complexes. *J. Mater. Chem.* **2012**, *22* (10), 4206−4215. (b) Lepeltier, M.; Dumur, F.; Wantz, G.; Vila, N.; Mbomekallé, I.; Bertin, D.; Gigmes, D.; Mayer, C. R. Red phosphorescent organic light-emitting diodes (PhOLEDs) based on a heteroleptic cyclometalated Iridium (III) complex. *J. Lumin.* **2013**, *143* (0), 145−149. (c) Chow, P.-K.; Cheng, G.; Tong, G. S. M.; To, W.-P.; Kwong, W.-L.; Low, K.-H.; Kwok, C.-C.; Ma, C.; Che, C.-M. Luminescent Pincer Platinum(II) Complexes with Emission Quantum Yields up to Almost Unity: Photophysics, Photoreductive C−C Bond Formation, and Materials Applications. *Angew. Chem., Int. Ed.* **2015**, *54* (7), 2084−2089.

(3) (a) Botchway, S. W.; Charnley, M.; Haycock, J. W.; Parker, A. W.; Rochester, D. L.; Weinstein, J. A.; Williams, J. A. G. Time-resolved and two-photon emission imaging microscopy of live cells with inert platinum complexes. *Proc. Natl. Acad. Sci. U. S. A.* **2008**, *105* (42), 16071−16076. (b) Liu, J.; Liu, Y.; Liu, Q.; Li, C.; Sun, L.; Li, F. Iridium(III) Complex-Coated Nanosystem for Ratiometric Upconversion Luminescence Bioimaging of Cyanide Anions. *J. Am. Chem. Soc.* **2011**, *133* (39), 15276−15279. (c) Li, C.; Yu, M.; Sun, Y.; Wu, Y.; Huang, C.; Li, F. A Nonemissive Iridium(III) Complex That Specifically Lights-Up the Nuclei of Living Cells. *J. Am. Chem. Soc.* **2011**, *133* (29), 11231−11239.

(4) (a) Fernandez-Moreira, V.; Thorp-Greenwood, F. L.; Coogan, M. P. Application of d_6 transition metal complexes in fluorescence cell imaging. *Chem. Commun.* **2010**, *46* (2), 186−202. (b) Baggaley, E.; Weinstein, J. A.; Williams, J. A. G. Lighting the way to see inside the live cell with luminescent transition metal complexes. *Coord. Chem. Rev.* **2012**, *256* (15−16), 1762−1785.

(5) Lo, K. K.-W.; Hui, W.-K.; Chung, C.-K.; Tsang, K. H.-K.; Ng, D. C.-M.; Zhu, N.; Cheung, K.-K. Biological labelling reagents and probes derived from luminescent transition metal polypyridine complexes. *Coord. Chem. Rev.* **2005**, *249* (13−14), 1434−1450.

(6) (a) Zhao, Q.; Yu, M.; Shi, L.; Liu, S.; Li, C.; Shi, M.; Zhou, Z.; Huang, C.; Li, F. Cationic Iridium(III) Complexes with Tunable Emission Color as Phosphorescent Dyes for Live Cell Imaging. *Organometallics* **2010**, *29* (5), 1085−1091. (b) Xiong, L.; Zhao, Q.; Chen, H.; Wu, Y.; Dong, Z.; Zhou, Z.; Li, F. Phosphorescence Imaging of Homocysteine and Cysteine in Living Cells Based on a Cationic Iridium(III) Complex. *Inorg. Chem.* **2010**, *49* (14), 6402−6408.

(7) Shi, H.; Sun, H.; Yang, H.; Liu, S.; Jenkins, G.; Feng, W.; Li, F.; Zhao, Q.; Liu, B.; Huang, W. Cationic Polyfluorenes with Phosphorescent Iridium(III) Complexes for Time-Resolved Luminescent Biosensing and Fluorescence Lifetime Imaging. *Adv. Funct. Mater.* **2013**, *23* (26), 3268−3276.

(8) Chen, Y.; Qiao, L.; Ji, L.; Chao, H. Phosphorescent iridium(III) complexes as multicolor probes for specific mitochondrial imaging and tracking. *Biomaterials* **2014**, *35* (1), 2−13.

(9) Lepeltier, M.; Lee, T. K.-M.; Lo, K. K.-W.; Toupet, L.; Le Bozec, H.; Guerchais, V. Synthesis and Photophysical Properties of Bis-Cyclometallated Iridium(III)−Styryl Complexes and Their Saturated Analogues. *Eur. J. Inorg. Chem.* **2007**, *2007* (18), 2734−2747.

(10) (a) Girardot, C.; Cao, B.; Mulatier, J.-C.; Baldeck, P. L.; Chauvin, J.; Riehl, D.; Delaire, J. A.; Andraud, C.; Lemercier, G. Ruthenium(II) Complexes for Two-Photon Absorption-Based Optical Power Limiting. *ChemPhysChem* **2008**, *9* (11), 1531−1535. (b) Natrajan, L. S.; Toulmin, A.; Chew, A.; Magennis, S. W. Two-photon luminescence from polar bis-terpyridyl-stilbene derivatives of Ir(III) and Ru(II). *Dalton Trans.* **2010**, *39* (45), 10837−10846. (c) Edkins, R. M.; Bettington, S. L.; Goeta, A. E.; Beeby, A. Two-photon spectroscopy of cyclometalated iridium complexes. *Dalton Trans.* **2011**, *40* (47), 12765−12770. (d) Massue, J.; Olesiak-Banska, J.; Jeanneau, E.; Aronica, C.; Matczyszyn, K.; Samoc, M.; Monnereau, C.; Andraud, C. Remarkable Effect of Iridium Cyclometalation on the Nonlinear Absorption Properties of a Quadrupolar Imine Ligand. *Inorg. Chem.* **2013**, *52* (19), 10705−10707. (e) Kim, K.-Y.; Farley, R. T.; Schanze, K. S. An Iridium(III) Complex that Exhibits Dual Mechanism Nonlinear Absorption. *J. Phys. Chem. B* **2006**, *110* (35), 17302−17304.

(11) Ho, M.-L.; Wang, J.-C.; Wang, T.-Y.; Lin, C.-Y.; Zhu, J. F.; Chen, Y.-A.; Chen, T.-C. The Construction of Glucose Biosensor Based on Crystalline Iridium(III)-Containing Coordination Polymers with Fiber-Optic Detection. *Sens. Actuators, B* **2014**, *190*, 479−485.

(12) Boreham, E. M.; Jones, L.; Swinburne, A. N.; Blanchard-Desce, M.; Hugues, V.; Terryn, C.; Miomandre, F.; Lemercier, G.; Natrajan, L. S. A cyclometallated fluorenyl Ir(III) complex as a potential sensitiser for two-photon excited photodynamic therapy (2PE-PDT). *Dalton Trans.* **2015**, *44*, 16127−16135.

(13) (a) Fan, Y.; Zhao, J.; Yan, Q.; Chen, P. R.; Zhao, D. Water-Soluble Triscyclometalated Organoiridium Complex: Phosphorescent Nanoparticle Formation, Nonlinear Optics, and Application for Cell Imaging. *ACS Appl. Mater. Interfaces* **2014**, *6* (5), 3122−3131. (b) He, L.; Tan, C.-P.; Ye, R.-R.; Zhao, Y.-Z.; Liu, Y.-H.; Zhao, Q.; Ji, L.-N.; Mao, Z.-W. Theranostic Iridium(III) Complexes as One- and Two-Photon Phosphorescent Trackers to Monitor Autophagic Lysosomes. *Angew. Chem., Int. Ed.* **2014**, *53* (45), 12137−12141. (c) Ho, C. L.; Wong, K. L.; Kong, H. K.; Ho, Y. M.; Chan, C. T. L.; Kwok, W. M.; Leung, K. S. Y.; Tam, H. L.; Lam, M. H. W.; Ren, X. F.; Ren, A. M.; Feng, J. K.; Wong, W. Y. A strong two-photon induced phosphorescent Golgi-specific in vitro marker based on a heteroleptic iridium complex. *Chem. Commun.* **2012**, *48* (19), 2525−2527. (d) Li, G.; Lin, Q.; Sun, L.; Feng, C.; Zhang, P.; Yu, B.; Chen, Y.; Wen, Y.; Wang, H.; Ji, L.; Chao, H. A mitochondrial targeted two-photon iridium(III) phosphorescent probe for selective detection of hypochlorite in live cells and in vivo. *Biomaterials* **2015**, *53*, 285−295.

(14) *APEX2*, Bruker AXS inc.: Madison, Wisconsin, USA, 2005.

(15) Sheldrick, G. M. *SADABS, program for scaling and correction of area detector data*, V2014/5; University of Göttingen, Germany, 1997.

(16) Blessing, R. H. *Acta Crystallogr., Sect. A: Found. Crystallogr.* **1995**, *51*, 33−38.

(17) Sheldrick, G. SHELXT - Integrated space-group and crystal-structure determination. *Acta Crystallogr., Sect. A: Found. Adv.* **2015**, *71* (1), 3−8.

(18) de Mello, J. C.; Wittmann, H. F.; Friend, R. H. An improved experimental determination of external photoluminescence quantum efficiency. *Adv. Mater.* **1997**, *9* (3), 230−232.

(19) Xu, C.; Webb, W. W. Measurement of Two-photon Excitation Cross Sections of Molecular Fluorophores with Data from 690 to 1050 nm. *J. Opt. Soc. Am. B* **1996**, *13*, 481−491.

(20) Rasband, W. S. *ImageJ* U.S. National Institutes of Health, Bethesda, Maryland, USA. http://rsb.info.nih.gov/ij/ 1997−2011.

(21) Peng, H.; Bria, A.; Zhou, Z.; Iannello, G.; Long, F. Extensible visualization and analysis for multidimensional images using Vaa3D. *Nat. Protoc.* **2014**, *9* (1), 193−208.

(22) Frisch, M. J.; Trucks, G. W.; Schlegel, H. B.; Scuseria, G. E.; Robb, M. A.; Cheeseman, J. R.; Scalmani, G.; Barone, V.; Mennucci, B.; Petersson, G. A.; Nakatsuji, H.; Caricato, M.; Li, X.; Hratchian, H. P.; Izmaylov, A. F.; Bloino, J.; Zheng, G.; Sonnenberg, J. L.; Hada, M.; Ehara, M.; Toyota, K.; Fukuda, R.; Hasegawa, J.; Ishida, M.; Nakajima, T.; Honda, Y.; Kitao, O.; Nakai, H.; Vreven, T.; Montgomery, J. A., Jr.; Peralta, J. E.; Ogliaro, F.; Bearpark, M.; Heyd, J. J.; Brothers, E.; Kudin, K. N.; Staroverov, V. N.; Kobayashi, R.; Normand, J.; Raghavachari, K.; Rendell, A.; Burant, J. C.; Iyengar, S. S.; Tomasi, J.; Cossi, M.; Rega, N.; Millam, J. M.; Klene, M.; Knox, J. E.; Cross, J. B.; Bakken, V.; Adamo, C.; Jaramillo, J.; Gomperts, R.; Stratmann, R. E.; Yazyev, O.;

DOI: 10.1021/acs.inorgchem.6b01253
Inorg. Chem. XXXX, XXX, XXX−XXX

Austin, A. J.; Cammi, R.; Pomelli, C.; Ochterski, J. W.; Martin, R. L.; Morokuma, K.; Zakrzewski, V. G.; Voth, G. A.; Salvador, P.; Dannenberg, J. J.; Dapprich, S.; Daniels, A. D.; Farkas, O.; Foresman, J. B.; Ortiz, J. V.; Cioslowski, J.; Fox, D. J. *Gaussian 09*, revision A.02; Gaussian, Inc.: Wallingford, CT, 2009.

(23) Adamo, C.; Barone, V. Toward reliable density functional methods without adjustable parameters: The PBE0 model. *J. Chem. Phys.* **1999**, *110* (13), 6158−6170.

(24) Le Bahers, T.; Bremond, E.; Ciofini, I.; Adamo, C. The nature of vertical excited states of dyes containing metals for DSSC applications: insights from TD-DFT and density based indexes. *Phys. Chem. Chem. Phys.* **2014**, *16* (28), 14435−14444.

(25) (a) Hariharan, P. C.; Pople, J. A. The influence of polarization functions on molecular orbital hydrogenation energies. *Theor. Chim. Acta* **1973**, *28* (3), 213−222. (b) Hay, P. J.; Wadt, W. R. Ab initio effective core potentials for molecular calculations. Potentials for the transition metal atoms Sc to Hg. *J. Chem. Phys.* **1985**, *82* (1), 270−283.

(26) Grimme, S.; Ehrlich, S.; Goerigk, L. Effect of the damping function in dispersion corrected density functional theory. *J. Comput. Chem.* **2011**, *32* (7), 1456−1465.

(27) Peach, M. J. G.; Tozer, D. J. Overcoming Low Orbital Overlap and Triplet Instability Problems in TDDFT. *J. Phys. Chem. A* **2012**, *116* (39), 9783−9789.

(28) Tomasi, J.; Mennucci, B.; Cammi, R. Quantum Mechanical Continuum Solvation Models. *Chem. Rev.* **2005**, *105* (8), 2999−3094.

(29) Barone, V.; Cossi, M. Quantum Calculation of Molecular Energies and Energy Gradients in Solution by a Conductor Solvent Model. *J. Phys. Chem. A* **1998**, *102* (11), 1995−2001.

(30) (a) Le Bahers, T.; Adamo, C.; Ciofini, I. A Qualitative Index of Spatial Extent in Charge-Transfer Excitations. *J. Chem. Theory Comput.* **2011**, *7* (8), 2498−2506. (b) Adamo, C.; Le Bahers, T.; Savarese, M.; Wilbraham, L.; García, G.; Fukuda, R.; Ehara, M.; Rega, N.; Ciofini, I. Exploring excited states using Time Dependent Density Functional Theory and density-based indexes. *Coord. Chem. Rev.* **2015**, *304*−*305*, 166−178.

(31) Santoro, F.; Improta, R.; Lami, A.; Bloino, J.; Barone, V. Effective Method to Compute Franck-Condon Integrals for Optical Spectra of Large Molecules in Solution. *J. Chem. Phys.* **2007**, *126* (8), 084509.

(32) (a) Nonoyama, M. Benzo[*h*]quinolin-10-yl-*N* Iridium(III) Complexes. *Bull. Chem. Soc. Jpn.* **1974**, *47* (3), 767−768. (b) Garces, F. O.; King, K. A.; Watts, R. J. Synthesis, structure, electrochemistry, and photophysics of methyl-substituted phenylpyridine ortho-metalated iridium(III) complexes. *Inorg. Chem.* **1988**, *27* (20), 3464−3471.

(33) Thomas Iii, S. W.; Yagi, S.; Swager, T. M. Towards chemosensing phosphorescent conjugated polymers: cyclometalated platinum(ii) poly(phenylene)s. *J. Mater. Chem.* **2005**, *15* (27−28), 2829−2835.

(34) Hudson, Z. M.; Wang, Z.; Helander, M. G.; Lu, Z.-H.; Wang, S. N-Heterocyclic Carbazole-Based Hosts for Simplified Single-Layer Phosphorescent OLEDs with High Efficiencies. *Adv. Mater.* **2012**, *24* (21), 2922−2928.

(35) Wang, X.-Y.; Kimyonok, A.; Weck, M. Functionalization of polymers with phosphorescent iridium complexes via click chemistry. *Chem. Commun.* **2006**, *37*, 3933−3935.

(36) Lepeltier, M.; Dumur, F.; Marrot, J.; Contal, E.; Bertin, D.; Gigmes, D.; Mayer, C. R. Unprecedented combination of regioselective hydrodefluorination and ligand exchange reaction during the syntheses of *tris*-cyclometalated iridium(III) complexes. *Dalton Trans.* **2013**, *42* (13), 4479−4486.

(37) (a) Lepeltier, M.; Lee, K.-M.; Lo, K.-W.-K.; Toupet, L.; Le Bozec, H.; Guerchais, V. Synthesis, Structure, and Photophysical and Electrochemical Properties of Cyclometallated Iridium(III) Complexes with Phenylated Bipyridine Ligands. *Eur. J. Inorg. Chem.* **2005**, *2005* (1), 110−117. (b) Neve, F.; Crispini, A. Metal-Containing Amphiphiles: Orthometallated Iridium(III) Complexes with Substituted 6′-Phenyl-2,2′-bipyridines. *Eur. J. Inorg. Chem.* **2000**, *2000* (5), 1039−1043.

(38) (a) Lamansky, S.; Djurovich, P.; Murphy, D.; Abdel-Razzaq, F.; Kwong, R.; Tsyba, I.; Bortz, M.; Mui, B.; Bau, R.; Thompson, M. E. Synthesis and Characterization of Phosphorescent Cyclometalated Iridium Complexes. *Inorg. Chem.* **2001**, *40* (7), 1704−1711. (b) Lamansky, S.; Djurovich, P.; Murphy, D.; Abdel-Razzaq, F.; Lee, H.-E.; Adachi, C.; Burrows, P. E.; Forrest, S. R.; Thompson, M. E. Highly Phosphorescent Bis-Cyclometalated Iridium Complexes: Synthesis, Photophysical Characterization, and Use in Organic Light Emitting Diodes. *J. Am. Chem. Soc.* **2001**, *123* (18), 4304−4312.

(39) Ipuy, M.; Liao, Y.-Y.; Jeanneau, E.; Baldeck, P. L.; Bretonniere, Y.; Andraud, C. Solid state red biphotonic excited emission from small dipolar fluorophores. *J. Mater. Chem. C* **2016**, *4* (4), 766−779.

(40) Talarico, A. M.; Aiello, I.; Bellusci, A.; Crispini, A.; Ghedini, M.; Godbert, N.; Pugliese, T.; Szerb, E. Highly luminescent bis-cyclometalated iridium(III) ethylenediamine complex: synthesis and correlation between the solid state polymorphism and the photophysical properties. *Dalton Trans.* **2010**, *39* (7), 1709−1712.

(41) Ahmad, Z.; Shah, A.; Siddiq, M.; Kraatz, H.-B. Polymeric micelles as drug delivery vehicles. *RSC Adv.* **2014**, *4* (33), 17028−17038.

(42) Maurin, M.; Vurth, L.; Vial, J.-C.; Baldeck, P.; Marder, S. R.; Sanden, B. V. d.; Stephan, O. Fluorescent Pluronic nanodots for in vivo two-photon imaging. *Nanotechnology* **2009**, *20* (23), 235102.

(43) (a) Matzinger, S.; Hussey, D. M.; Fayer, M. D. Fluorescent Probe Solubilization in the Headgroup and Core Regions of Micelles: Fluorescence Lifetime and Orientational Relaxation Measurements. *J. Phys. Chem. B* **1998**, *102* (37), 7216−7224. (b) Monnereau, C.; Marotte, S.; Lanoe, P.-H.; Maury, O.; Baldeck, P. L.; Kreher, D.; Favier, A.; Charreyre, M.-T.; Marvel, J.; Leverrier, Y.; Andraud, C. Water-soluble chromophores with star-shaped oligomeric arms: synthesis, spectroscopic studies and first results in bio-imaging and cell death induction. *New J. Chem.* **2012**, *36* (11), 2328−2333.

(44) Xu, C.; Webb, W. W. Measurement of two-photon excitation cross sections of molecular fluorophores with data from 690 to 1050 nm. *J. Opt. Soc. Am. B* **1996**, *13* (3), 481−491.

(45) Note that the reported value is given per iridium complex and not per nanoparticle. We chose to use this convention because a precise estimation of the number of complexes per nanoparticle is difficult.

(46) Massin, J.; Charaf-Eddin, A.; Appaix, F.; Bretonniere, Y.; Jacquemin, D.; van der Sanden, B.; Monnereau, C.; Andraud, C. A water soluble probe with near infrared two-photon absorption and polarity-induced fluorescence for cerebral vascular imaging. *Chem. Sci.* **2013**, *4* (7), 2833−2843.

(47) (a) Yang, G.; Pan, F.; Parkhurst, C. N.; Grutzendler, J.; Gan, W.-B. Thinned-skull cranial window technique for long-term imaging of the cortex in live mice. *Nat. Protoc.* **2010**, *5* (2), 201−208. (b) Mettra, B.; Appaix, F.; Olesiak-Banska, J.; Le Bahers, T.; Leung, A.; Matczyszyn, K.; Samoc, M.; van der Sanden, B.; Monnereau, C.; Andraud, C. A Fluorescent Polymer Probe with High Selectivity toward Vascular Endothelial Cells for and beyond Noninvasive Two-Photon Intravital Imaging of Brain Vasculature. *ACS Appl. Mater. Interfaces* **2016**, *8* (27), 17047−17059.

(48) Ding, D.; Goh, C. C.; Feng, G.; Zhao, Z.; Liu, J.; Liu, R.; Tomczak, N.; Geng, J.; Tang, B. Z.; Ng, L. G.; Liu, B. Ultrabright Organic Dots with Aggregation-Induced Emission Characteristics for Real-Time Two-Photon Intravital Vasculature Imaging. *Adv. Mater.* **2013**, *25* (42), 6083−6088.

DOI: 10.1021/acs.inorgchem.6b01253
Inorg. Chem. XXXX, XXX, XXX−XXX